East Asian Journal on Applied Mathematics
doi: 10.4208/eajam.2023-227.221023

Vol. **xx**, No. x, pp. 1-22
2024

Analysis of Irreversibility in the Flow of Jeffrey Fluid Through an Inclined Channel Considering Navier-Slip

Ravi Mahla and Kolla Kaladhar*

Department of Mathematics, National Institute of Technology, Warangal 506004, India.

Received 14 September 2023; Accepted (in revised version) 22 October 2023.

Abstract. In this paper, we investigate the phenomenon of entropy generation of natural convection Jeffrey fluid flow through a sloping channel under Navier-Slip conditions. The study considers the influences of the Soret effect, inclined magnetic field, and Hall current. Employing appropriate transformations, we express the main equations in dimensionless form. Numerical solutions are implemented using the spectral quasi-linearization method (SQLM). Graphical representations are utilized to assess the impacts of diverse thermophysical parameters. Empirical findings indicate that augmenting the channel inclination angle, inclination angle, Soret number, and magnetic parameter induces a proportional rise in entropy generation. Conversely, a surge in Hall current yields a reduction in entropy generation. When the Soret parameter, magnetic parameter, channel inclination angle, and Jeffrey fluid parameter increase, it increases flow and cross-flow velocity. A contrary trend is observed for the Hall parameter.

AMS subject classifications: 76R10, 76W05, 37M25, 81V70, 78M22

Key words: Natural convection, inclined magnetic field, sloping channel, Entropy, SQLM.

1. Introduction

Natural convection in enclosures draws attention with its many applications in various fields, encompassing lead-acid batteries, thermal storage, solar collectors, food, and drying technologies. This process is synonymous with natural heat convection and is driven by buoyancy disparities induced by temperature gradients. Engineers harness natural convection flows occurring between vertically oriented parallel walls for diverse purposes, such as cooling electronic equipment, devising heat exchangers, operating nuclear reactors, exploiting solar energy, and implementing geothermal systems, among other industrial endeavors [8,10,12,19,40,43]. Researchers in fluid mechanics and heat transfer have extensively probed these flows due to their paramount significance in the relevant sector.

*Corresponding author. *Email addresses:* kaladhar@nitw.ac.in (K. Kaladhar), rm712151@student.nitw.ac.in (R. Mahla)

The exploration of natural convection phenomena provides valuable insights for optimizing technology and advancing engineering applications in an energy-efficient and sustainable manner. Hajizadeh *et al.* [14] studied the unforced convective flow of a nanofluid between vertically aligned parallel plates. Tanveer *et al.* [39] investigated the free convection flows of nanofluids by taking the generalized fractional thermal flux into account. Recently, Ali *et al.* [2] investigated the synergistic influence of heat transfer and a magnetic field on the phenomenon of free convection in magneto-hydrodynamic (MHD) Casson fluid flow occurring between parallel plates. Most recently, Bako and Ajibade [3] explored the impacts of g-jitter on natural convection Couette flow within a vertical channel.

The Soret effect, a phenomenon where a mass flux is induced by a temperature difference, plays a crucial role in various physical processes and finds applications in fields such as geosciences and chemical engineering [33, 38]. Mandal *et al.* [24] conducted a study utilizing an inclined stretching plate with different surface conditions to investigate the characteristics of the Soret effect and its interaction with magnetohydrodynamics. Mishra *et al.* [25] focused on the impact of Soret diffusion in hydromagnetically mixed convective flow passing through the center of infinite vertical plates. Recently, Agrawal *et al.* [1] conducted research into the influence of Soret number in conjunction with Hall parameter and induced magnetic field effects on combined convection flow through vertical channels. The objective of this study was to elucidate how the interplay between the Soret effect and magnetic forces affects flow characteristics and heat transfer phenomena. Most recently, Hamza *et al.* [15] investigated the heat transfer flow in natural convection controlled by the Arrhenius equation, influenced by an induced magnetic field within a micro-channel.

Fluid flows with slip at boundaries indeed have significant implications for various micro and macroscopic devices, including applications such as surface polishing. In 1823, Navier [29] introduced a slip boundary condition, stating that the velocity at the interface between a solid and a fluid is linearly affected by shear stress. Building upon Navier's work, Das *et al.* [9] presented the findings of their research, which focused on slip flow through sloping porous channel. In their study, the authors considered the influences of viscous dissipation and joule heating within the fluid flow. Filahi *et al.* [11] investigated the thermosolutal convection within a horizontal porous layer containing a binary fluid influenced by the Soret effect. Gjerde and Scott [13] conducted a study to examine the instability in kinetic energy within fluid flows subject to slip boundary conditions. Recently, Bernatchou *et al.* [6] analyzed the impact of a magnetic field on double diffusive free convection occurring within an inclined enclosure that contains a nanofluid. The study also encompassed consideration of the Soret number's influence. Most recently, Raghunath [36] conducted an investigation into the heat and mass transfer characteristics of nanofluid flow based on water over a stretching sheet. The study also considered the impact of thermal radiation, magnetic field, and Soret number.

Non-Newtonian fluids find diverse applications spanning industries such as food, pharmaceutics, paints, coatings, and polymer processing. In recent decades, there has been extensive discourse concerning the rheological attributes of non-Newtonian fluids, which captivates researchers. The Jeffrey fluid, as expounded in references [17,18,28,42], stands among various models utilized for elucidating the conduct and properties of these fluids.

The Jeffrey fluid model has garnered utilization across diverse domains, including polymer processing, biomechanics, and rheology. It furnishes a mathematical framework facilitating the explication of intricate viscoelastic tendencies in non-Newtonian fluids. This framework empowers researchers and engineers to comprehend and prognosticate the flow characteristics of such fluids in assorted scenarios. Some applications of Jeffrey fluid are the peristaltic flow of chyme in the small intestine, almost all industrial fluids such as paints, paper pulp, toothpaste, vasomotion of small blood vessels, and swallowing food through the esophagus. In this fluid, there is an extrinsic connection between stress and strain rate. It explains the concepts of retardation and relaxation time. The constitutive equation for the extra stress tensor in Jeffrey fluid is defined by [16]

$$\overline{S} = \frac{\mu}{1+\lambda_1}(\dot{\gamma} + \lambda_2 \ddot{\gamma}).$$

In the above equation, λ_1 is the ratio of relaxation to retardation times, $\dot{\gamma}$ is the shear rate, λ_2 is the retardation time, and $\ddot{\gamma}$ is the differentiation of shear rate with respect to time. The Jeffrey model is recognized as a generalization of the frequently used Newtonian fluid model because its constitutive equation can be reduced to that of the Newtonian model as a special case. Ojjela *et al.* [30] delved into the exploration of how a magnetic field and radiation impact the natural convection flow of a Jeffrey fluid between parallel plates in a porous medium under the impact of the Dufour and Soret parameter. Khan *et al.* [22] delved into the analysis of a generalized two-phase Jeffrey fluid flow through a vertical channel, encompassing considerations of heat transfer. Recently, Omokhuale and Dange [31] explored the influence of heat absorption on the convective flow of a Jeffrey fluid, with an emphasis on an infinite vertical plate. Most recently, Kodi *et al.* [23] examined the unsteady MHD flow of a Jeffrey fluid through porous media, considering the inclusion of thermal radiation, Hall current, and Soret effects. However, the Jeffrey fluid flow model has its drawbacks. One of these limitations is its applicability restricted to low Reynolds number flows. When the Reynolds numbers are high and the flow becomes turbulent, the Jeffrey fluid flow model becomes inadequate for accurately predicting the flow behavior.

In the realm of thermodynamics, the concept of entropy generation plays a pivotal role in assessing the irreversibility and energy dissipation inherent to various energy conversion processes. It serves as a crucial indicator for evaluating the efficiency and sustainability of diverse thermodynamic systems. Rooted in the Second Law of Thermodynamics, which asserts the inevitable increase in the total entropy of a closed system during energy transformations, entropy generation quantifies the extent to which useful energy is lost and dispersed. A central metric within entropy generation analysis is the entropy generation rate, which measures the rate at which irreversibilities manifest within a system. The pursuit of minimizing entropy generation stands as a key objective in engineering and scientific disciplines, signifying enhanced energy efficiency and reduced environmental impact. Researchers and engineers employ entropy generation analysis as a strategic tool for optimizing system design and elevating overall performance in various domains encompassing heat transfer, fluid dynamics, and process engineering. Bejan *et al.* [32] originally established the idea of entropy generation minimization, which was initially used to describe industrial

thermal systems. Chamkha *et al.* [7] examined the phenomenon of entropy production in conjunction with natural convection occurring within a C-shaped enclosure that contains a nanofluid and is subjected to the influence of a magnetic field. Pordanjani *et al.* [35] explored the dynamics of natural convection heat transfer and generation of entropy within a cavity. This cavity is subjected to the presence of a nanofluid flow and is further influenced by thermal radiation and magnetic field. Recently, Balamurugan *et al.* [4] examined the entropy production of natural and forced convection flow within a porous channel. Additionally, the system is subject to the effect of an aligned magnetic field and incorporates Navier slip conditions. Most recently, Kaladhar and Ravi [20] explored the entropy generation associated with the flow of a Jeffrey fluid between vertical parallel plates, taking into account the influence of an angled magnetic field and adhering to Navier-Slip conditions.

The prevailing portion of the research detailed in the cited literature focuses on the context of parallel plate geometry, which deals with viscous fluids, nanofluids, Casson fluids, and Jeffrey fluids. However, there has been a noticeable lack of emphasis on the analysis of entropy generation in Jeffrey fluid related to sloping channel geometry with an inclined magnetic field. This research addresses this gap by focusing on the examination of the entropy analysis of Jeffrey fluid with Navier-Slip boundary conditions and considering a sloping channel subjected to an inclined magnetic field by including various physical effects. It is noteworthy that no prior work has been undertaken to explore the intricacies of the entropy generation of Jeffrey fluid flow under Navier-Slip conditions. Use SQLM to solve dimensionless equations. Bellman *et al.* [5] introduced the quasi-linearization method as a simplified version of the Newton-Raphson technique. Motsa *et al.* [27] investigated the utilization of SQLM to address unsteady boundary layer flow issues. Srinivas *et al.* [37] employed the SQLM method to explore entropy generation in a tangent hyperbolic fluid within the context of the quadratic Boussinesq approximation. Kaladhar and Ravi [21] utilized SQLM to investigate the effect of the inclined magnetic field, Hall current, and Soret number on mixed convection flow between vertical parallel plates. Recently, Zare *et al.* [44] applied SQLM to numerically solve non-standard Volterra integral equations.

2. Mathematical Modeling

The physical arrangement depicted in Fig. 1 of this research comprises a pair of inclined parallel plates. These plates form an angle γ with the reference base and are separated by a distance of $2d$. The phenomenon of slip is taken into account on both of these plates. The concentrations and temperatures at the plates are denoted as C_1, T_1, C_2, and T_2, respectively. An external magnetic field B_0, oriented at an angle α concerning the base, exerts an influence on the plates. In this problem, we examine the consistent and incompressible flow of a Jeffrey fluid driven by natural convection. Given that the boundaries extend infinitely along the x-axis, the flow parameters are presumed to be solely functions of the coordinate y. Except for the impact of changes in density on the buoyancy force term, the fluid properties are considered constant. As such, these assumptions align with natural principles and are relevant in practical applications.

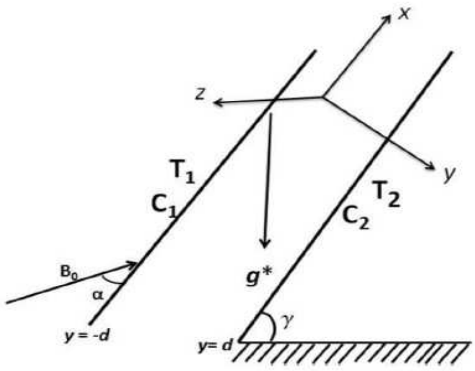

Figure 1: Physical interpretation.

In this particular rendition, the governing equations are established as follows:

$$\frac{\partial v}{\partial y} = 0 \Rightarrow v = v_0 = \text{constant},$$

$$\rho v_0 \frac{\partial u}{\partial y} = \rho g^* \sin\gamma\big(\beta_T(T-T_1)+\beta_C(C-C_1)\big) + \frac{\mu}{1+\lambda_1}\frac{\partial^2 u}{\partial y^2} - \frac{\sigma B_0^2 \cos\alpha}{1+m^2\cos^2\alpha}\big(u\cos\alpha - v_0\sin\alpha + mw\cos^2\alpha\big), \tag{2.1}$$

$$\rho v_0 \frac{\partial w}{\partial y} = -\rho g^* \cos\gamma\big(\beta_T(T-T_1)+\beta_C(C-C_1)\big) + \frac{\mu}{1+\lambda_1}\frac{\partial^2 w}{\partial y^2} + \frac{\sigma B_0^2 \cos^2\alpha}{1+m^2\cos^2\alpha}(mu\cos\alpha - w - mv_0\sin\alpha), \tag{2.2}$$

$$\rho c_p v_0 \frac{\partial T}{dy} = k_f \frac{\partial^2 T}{\partial y^2} + \frac{\mu}{1+\lambda_1}\left(\left(\frac{\partial u}{\partial y}\right)^2 + \left(\frac{\partial w}{\partial y}\right)^2\right), \tag{2.3}$$

$$v_0 \frac{\partial C}{\partial y} = D\frac{\partial^2 C}{\partial y^2} + \frac{DK_T}{T_m}\frac{\partial^2 T}{\partial y^2} \tag{2.4}$$

with

$$\begin{aligned} u &= \gamma_1 \frac{\partial u}{\partial y}, \quad w = 0, \quad C = C_1, \quad T = T_1, \quad \text{when} \quad y = -d, \\ u &= \gamma_2 \frac{\partial u}{\partial y}, \quad w = 0, \quad C = C_2, \quad T = T_2, \quad \text{when} \quad y = d, \end{aligned} \tag{2.5}$$

where λ_1 is the Jeffrey fluid parameter, K_T the ratio of thermal diffusion, c_P a specific heat, k_f is the thermal conductivity, μ the viscosity coefficient, $m = \zeta_1 \sigma B_0$ the Hall parameter with the Hall factor ζ_1, ρ the density, σ the electrical conductivity, D the mass dissipation, T_m the mean temperature, and g^* the gravitational acceleration. Besides, γ_1, γ_2 are coefficients associated with the slip conditions, and β_T and β_C are the coefficients characterizing the thermal and solutal expansion, respectively.

To attain the dimensionless formulation of the aforementioned system, the subsequent dimensionless transformations are taken into consideration

$$y=\eta d,\quad u=\nu Grf/d,\quad w=\nu Grg/d,\quad C-C_1=(C_2-C_1)\phi,\quad T-T_1=(T_2-T_1)\theta.$$

By applying the dimensionless transformations to the Eqs. (2.1) through (2.5), we yield the resulting transformed equations as follows:

$$\begin{aligned}
&f''-Re(1+\lambda_1)f'+(1+\lambda_1)(\theta+N\phi)\sin\gamma\\
&\quad-\frac{Ha^2\cos\alpha(1+\lambda_1)}{1+m^2\cos^2\alpha}\left(f\cos\alpha-\lambda\sin\alpha+mg\cos^2\alpha\right)=0, &(2.6)\\
&g''-Re(1+\lambda_1)g'+(1+\lambda_1)(\theta+N\phi)\cos\gamma\\
&\quad+\frac{Ha^2\cos^2\alpha(1+\lambda_1)}{1+m^2\cos^2\alpha}(mf\cos\alpha-g-m\lambda\sin\alpha)=0, &(2.7)\\
&\theta''-RePr\theta'+\frac{BrGr^2}{(1+\lambda_1)}\left(f'^2+g'^2\right)=0, &(2.8)\\
&\phi''-ReSc\phi'+ScSr\theta''=0 &(2.9)
\end{aligned}$$

with

$$\begin{aligned}
&f(-1)=\beta_1 f'(-1),\quad g(-1)=0,\quad \phi(-1)=0,\quad \theta(-1)=0.\\
&f(1)=\beta_2 f'(1),\qquad g(1)=0,\qquad \phi(1)=1,\qquad \theta(1)=1,
\end{aligned}\tag{2.10}$$

where $Br=\mu\nu^2/k_f d^2(T_2-T_1)$ is the Brinkman number, $Sr=DK_T(T_2-T_1)/\nu T_m(C_2-C_1)$ the Soret number, $Re=\rho u_0 d/\mu$ the Reynolds number, $Sc=\nu/D$ the Schmidth number, $Gr=g^*\beta_T(T_2-T_1)d^3/\nu^2$ the Grashof number, $Ha=dB_0\sqrt{\sigma/\mu}$ the magnetic parameter, $Pr=\mu c_p/k_f$ the Prandtl number, $N=\beta_C(C_2-C_1)/\beta_T(T_2-T_1)$ the buoyancy parameter, $\lambda=Re/Gr$, and $\beta_1=\gamma_1/d$, $\beta_2=\gamma_2/d$ are the slip parameters.

The shear stress, heat, and mass flows can be obtained from

$$\tau_w=\mu\frac{du}{dy}\Big|_{y=\pm d},\quad q_w=-k_f\frac{dT}{dy}\Big|_{y=\pm d},\quad q_m=-D\frac{dC}{dy}\Big|_{y=\pm d}.$$

Dimensionless forms of skin friction coefficient $C_f=\tau_w/\rho u_0^2$, Nusselt number $Nu=q_w d/k_f(T_2-T_1)$, and the Sherwood number $Sh=q_m d/D(C_2-C_1)$ are given by

$$ReC_{f_1}=f'(-1),\quad ReC_{f_2}=f'(1),\quad Nu_{1,2}=-\theta'(\eta)\big|_{\eta=-1,1},\quad Sh_{1,2}=-\phi'(\eta)\big|_{\eta=-1,1}.$$

3. Spectral Quasi-linearization Method

The spectral quasi-linearization method is used to numerically solve a set of coupled non-linear equations (2.6)-(2.9) with boundary condition (2.10). This technique enhances the stability and accuracy of the Bellman-Kalaba [5] quasi-linearization method by combining it with the extraordinary accuracy of spectral collocation. With this approach, the iteration scheme is created by linearizing the differential equation with the help of Taylor

series expansion. Next, applying the SQLM to Eqs. (2.6)-(2.9) by assuming the approximate solution f_r, g_r, θ_r, and ϕ_r, and f_{r+1} , g_{r+1} , θ_{r+1} and ϕ_{r+1} be improved solution. The following describes an iterative model based on SQLM:

$$\begin{aligned}
&f''_{k+1} - Re(1+\lambda_1)f'_{k+1} + (1+\lambda_1)(\theta_{k+1} + N\phi_{k+1})\sin\gamma + a_1 f_{k+1} + a_2 g_{k+1} = a_3,\\
&g''_{k+1} - Re(1+\lambda_1)g'_{k+1} - (1+\lambda_1)(\theta_{k+1} + N\phi_{k+1})\cos\gamma + a_4 f_{k+1} + a_5 g_{k+1} = a_6,\\
&\theta''_{r+1} - RePr\,\theta'_{r+1} + a_7 f'_{k+1} + a_8 g'_{k+1} = a_9,\\
&\phi''_{r+1} - ReSc\,\phi'_{r+1} + ScSr\,\theta''_{r+1} = 0,
\end{aligned} \tag{3.1}$$

where

$$\begin{aligned}
a_1 &= -\frac{Ha^2(1+\lambda_1)\cos^2\alpha}{1+m^2\cos^2\alpha}, & a_2 &= -\frac{mHa^2(1+\lambda_1)\cos^3\alpha}{1+m^2\cos^2\alpha},\\
a_3 &= -\frac{\lambda Ha^2(1+\lambda_1)\cos\alpha\sin\alpha}{1+m^2\cos^2\alpha}, & a_4 &= \frac{mHa^2\cos^3\alpha(1+\lambda_1)}{1+m^2\cos^2\alpha},\\
a_5 &= -\frac{Ha^2(1+\lambda_1)\cos^2\alpha}{1+m^2\cos^2\alpha}, & a_6 &= \frac{\lambda mHa^2\cos^2\alpha\sin\alpha(1+\lambda_1)}{1+m^2\cos^2\alpha},\\
a_7 &= \frac{2BrGr^2}{1+\lambda_1}f'_k, \quad a_8 = \frac{2BrGr^2}{1+\lambda_1}g'_k, & a_9 &= \frac{BrGr^2}{(1+\lambda_1)}\left(f'^2_k + g'^2_k\right).
\end{aligned}$$

The preceding system (3.1) is an iterative system of linear differential equations with variable coefficients solved for $r = 0, 1, 2, \ldots$. The quasi-linearization scheme in this study was solved using the Chebyshev pseudo-spectral approach. The iteration procedures (3.1) can be solved step by step for $F_{r+1}(\eta)$, $G_{r+1}(\eta)$, $\Theta_{r+1}(\eta)$, and $\Phi_{r+1}(\eta)$, with r taking the values with initial approximations f_0, g_0, θ_0, and ϕ_0. To solve Eqs. (3.1), we discretize them and utilize the Chebyshev spectral collocation method. This method employs a differential matrix, denoted as D, to approximate the derivatives of the unknown functions $f(\eta)$, $g(\eta)$, $\theta(\eta)$, and $\phi(\eta)$ at the N_x collocated points

$$\eta_j = \cos\left(\frac{j\pi}{N_x}\right), \quad j = 0, 1, 2, 3, \ldots, N_x$$

and leads to the matrix equation

$$\mathbf{A}_r\mathbf{X}_{r+1} = \mathbf{B}_r,$$

where $\mathbf{A}_r$ is a $(4N_x+4)\times(4N_x+4)$ square matrix, $\mathbf{X}_r$ and $\mathbf{B}_r$ are column matrices of size $(4N_x+4)\times 1$, and are defined as

$$\begin{aligned}
\mathbf{A}_r &= \begin{bmatrix} A_{11} & A_{12} & A_{13} & A_{14}\\ A_{21} & A_{22} & A_{23} & A_{24}\\ A_{31} & A_{32} & A_{33} & A_{34}\\ A_{41} & A_{42} & A_{43} & A_{44}\end{bmatrix},\\
\mathbf{X}_{r+1} &= \begin{bmatrix}\mathbf{F}_{k+1} & \mathbf{G}_{k+1} & \boldsymbol{\Theta}_{k+1} & \boldsymbol{\Phi}_{k+1}\end{bmatrix}^T,\\
\mathbf{B}_r &= \begin{bmatrix}\mathbf{K}_1 & \mathbf{K}_2 & \mathbf{K}_3 & \mathbf{K}_4\end{bmatrix}^T,
\end{aligned}$$

where

$$\begin{aligned}
&\mathbf{F}_{k+1} = \left[f_{r+1}(\xi_0), f_{r+1}(\xi_1), \ldots, f_{r+1}(\xi_{N_x})\right]^T,\\
&\mathbf{G}_{k+1} = \left[g_{r+1}(\xi_0), g_{r+1}(\xi_1), \ldots, g_{r+1}(\xi_{N_x})\right]^T,\\
&\mathbf{\Theta}_{k+1} = \left[\theta_{r+1}(\xi_0), \theta_{r+1}(\xi_1), \ldots, \theta_{r+1}(\xi_{N_x})\right]^T,\\
&\mathbf{\Phi}_{k+1} = \left[\phi_{r+1}(\xi_0), \phi_{r+1}(\xi_1), \ldots, \phi_{r+1}(\xi_{N_x})\right]^T,\\
&\mathbf{K}_1 = \left[a_3(\xi_0), a_3(\xi_1), \ldots, a_3(\xi_{N_x})\right]^T,\\
&\mathbf{K}_2 = \left[a_6(\xi_0), a_6(\xi_1), \ldots, a_6(\xi_{N_x})\right]^T,\\
&\mathbf{K}_3 = \left[a_9(\xi_0), a_9(\xi_1), \ldots, a_9(\xi_{N_x})\right]^T,\\
&\mathbf{K}_4 = O,\\
&A_{11} = D^2 - Re(1+\lambda_1)D + a_1, \quad A_{12} = a_2,\\
&A_{13} = \sin\gamma(1+\lambda_1) * I, \quad A_{14} = \sin\gamma(1+\lambda_1) * N * I,\\
&A_{21} = a_4, \quad A_{22} = D^2 - Re(1+\lambda_1)D + a_5,\\
&A_{23} = \cos\gamma(1+\lambda_1) * I, \quad A_{24} = \cos\gamma(1+\lambda_1) * N * I,\\
&A_{31} = a_7 D, \quad A_{32} = a_8 D, \quad A_{33} = D^2 - RePrD, \quad A_{34} = O,\\
&A_{41} = O, \quad A_{42} = O, \quad A_{43} = ScSrD^2, \quad A_{44} = D^2 - ReScD.
\end{aligned}$$

Here, I and O represents the identity and zero matrix of size $(N_x+1)\times(N_x+1)$. The approximations for f, g, θ, and ϕ are obtained as follows:

$$\mathbf{X}_{r+1} = \mathbf{A}_r^{-1}\mathbf{B}_r.$$

4. Entropy Generation

In the field of thermal equipment design, the meticulous analysis of entropy generation is crucial because it plays a vital role in improving the efficiency of ongoing thermal processes. In accordance with the established principles of thermodynamics, the process of heat transfer within a system leads to results such as thermodynamic reversibility and the simultaneous appearance of entropy. As a corollary, the scrutiny of entropy production in scenarios involving fluid flow coupled with heat transfer becomes imperative, necessitating the inclusion of irreversibility within the purview of thermodynamic investigations. By the second law of thermodynamics, the expression for the rate of volumetric entropy production [26, 34, 41] is given as

$$\begin{aligned}
S_{gen} = {} & \frac{k_f}{T_0^2}\left[\frac{dT}{dy}\right]^2 + \frac{\mu}{T_0(1+\lambda_1)}\left[\left(\frac{du}{dy}\right)^2 + \left(\frac{dw}{dy}\right)^2\right] + \frac{RD}{C_0}\left(\frac{dC}{dy}\right)^2\\
& + \frac{RD}{T_0}\left(\frac{dT}{dy}\right)\left(\frac{dC}{dy}\right) + \frac{\sigma B_0^2}{T_0}\left[w^2 + (u\cos\alpha - v_0\sin\alpha)^2\right]. \qquad (4.1)
\end{aligned}$$

The initial expression on the right-hand side of Eq. (4.1) is linked to heat transfer; the subsequent term is indicative of viscous dissipation; the third and fourth terms represent mass transfer; the fifth term is due to applied magnetic field

$$(S_{gen})_0 = \frac{k_f (T_2 - T_1)^2}{T_0^2 d^2}. \tag{4.2}$$

Using the Eqs. (4.1) and (4.2), we express the formation of dimensionless entropy as

$$N_s = \frac{S_{gen}}{(S_{gen})_0},$$

$$N_s = (\theta')^2 + \frac{BrGr^2}{(1+\lambda_1)A_1}(f'^2 + g'^2) + \frac{\varepsilon B_1^2}{A_1^2}(\phi')^2 + \frac{\varepsilon B_1}{A_1}\theta'\phi' + \frac{BrGr^2 Ha^2}{A_1}\left(g^2 + (f\cos\alpha - \lambda\sin\alpha)^2\right).$$

Here, $Br, \varepsilon, B_1, Gr, Ha$, and A_1 correspond to the Brinkman number, dimensionless constant parameter, dimensionless concentration difference, Grashof number, Hartman number, and dimensionless temperature difference, respectively, which are represented as

$$Br = \frac{\mu v^2}{k_f d^2 (T_2 - T_1)}, \quad Gr = \frac{g^* \beta_T (T_2 - T_1) d^3}{v^2}, \quad \varepsilon = \frac{RDC_0}{k_f},$$

$$A_1 = \frac{T_2 - T_1}{T_0}, \quad B_1 = \frac{C_2 - C_1}{C_0}, \quad Ha = dB_0\sqrt{\frac{\sigma}{\mu}}.$$

5. Result and Discussion

The analytical solutions corresponding to Eqs. (2.6), (2.8), and (2.9), along with their boundary conditions (2.10), were deduced while excluding the consideration of certain parameters, namely the Brinkman number (Br), Soret parameter (Sr), channel inclination angle (γ), magnetic parameter (Ha), and Jeffrey fluid parameter (λ_1) with an inclination angle of $\alpha = 45$. These solutions are compared to those implemented using SQLM, as shown in the Table 1. Comparative results showed high agreement. Therefore, SQLM code can be safely used to explore the topics covered in this study.

Figs. 2-9 show the behaviour of $f(\eta), g(\eta), \theta(\eta), \phi(\eta)$, and Ns for distinct values of $Ha, \alpha, m, Sr, \lambda_1, \gamma, \beta_1$, and β_2 by taking $Gr, N, Sc, Pr, Br, Re, A_1, B_1, \varepsilon, \beta_1, \beta_2$ at 2, 2, 0.22, 0.71, 0.5, 2, 1, 1, 2, 0.1, 0.1, respectively.

In Fig. 2, the variations in f, g, θ, ϕ, and Ns are depicted across different values of magnetic parameter (Ha), while $Sr = 2$, $\alpha = \pi/4$, $m = 2$, $\lambda_1 = 0.5$, and $\gamma = \pi/3$ are held constant. Figs. 2(a) and 2(b) exhibit the discernible augmentation of both flow velocity and cross-flow velocity with the progressive elevation of the magnetic parameter (Ha). It is noteworthy to highlight that the magnetic field is inclined at an angle $\alpha > 0$, leading to the absence of drag force generation. Figs. 2(c) and 2(d) demonstrate the concurrent

Table 1: Comparison of the SQLM solution with the analytical solution is conducted in the scenario where $\lambda_1 = 0, Br = 0, Sr = 0, \gamma = 0$, and Ha=0.

η	f		θ		ϕ	
	Analytical	SQLM	Analytical	SQLM	Analytical	SQLM
-1	0.183670	0.183673	0	0	0	0
-0.5	0.270749	0.270747	0.0625502	0.0625501	0.170905	0.1709047
0	0.317368	0.317365	0.194662	0.1946615	0.391741	0.3917409
0.5	0.399532	0.399535	0.466847	0.4668472	0.668017	0.6680167
1	-0.224485	-0.224489	1	1	1	1

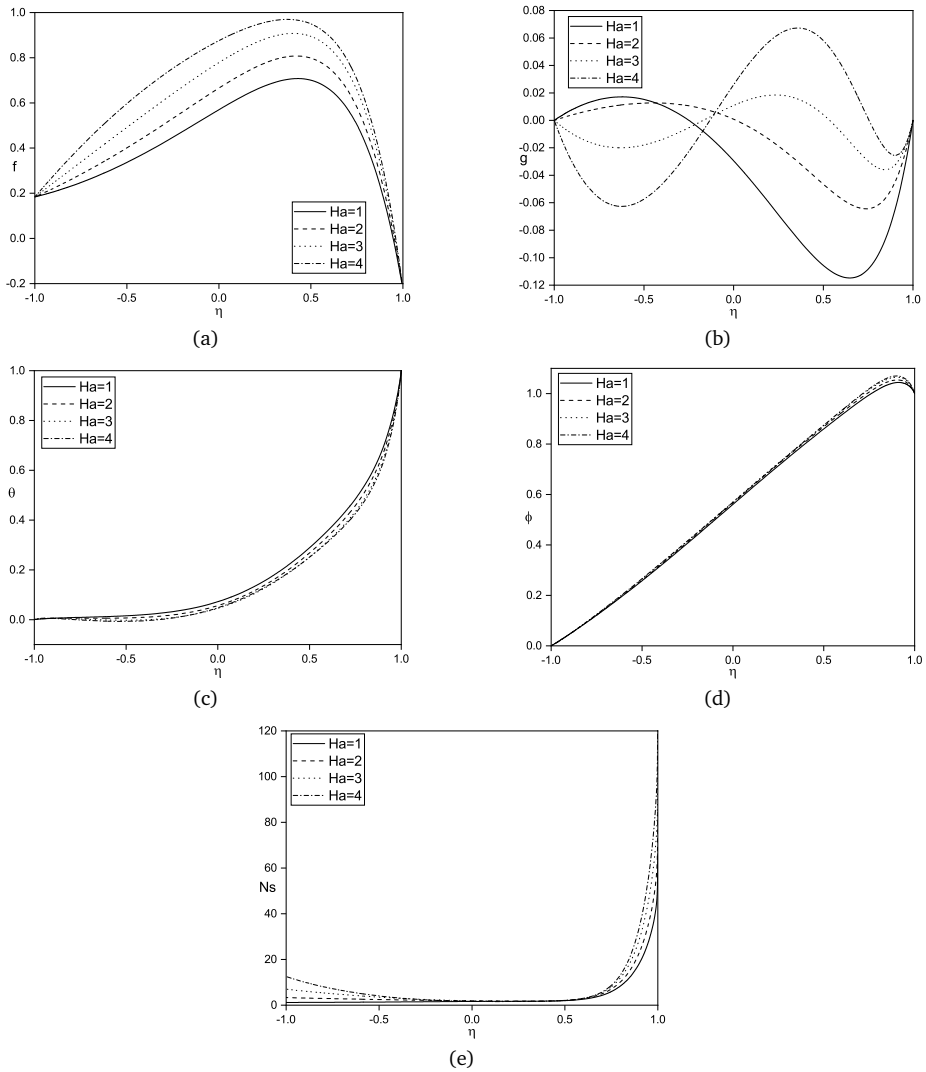

Figure 2: Effect of Ha on (a): $f(\eta)$, (b): $g(\eta)$, (c): $\theta(\eta)$, (d): $\phi(\eta)$, and (e): Ns.

behavior of subsidence in fluid temperature and magnifies in concentration with elevated values of Ha. It is seen in Fig. 2(e) that entropy magnifies near the plates as Ha magnifies. Fluid dynamics can be influenced by a magnetic field owing to the magneto-hydrodynamic (MHD) phenomenon, which holds particular importance in the context of fluids that exhibit electrical conductivity. Magnetic parameters play a crucial role in power generation systems where a conducting fluid interacts with a magnetic field to generate electric power, high-speed trains, magnetic resonance imaging, paleomagnetism, metal sorting, etc.

In Fig. 3, the depictions illustrate the response of parameters f, g, θ, ϕ, and Ns regarding discrete orientations of the inclination angle (α), while keeping $Ha = 2, m = 2, \lambda_1 = 0.1, Sr = 2$, and $\gamma = \pi/3$ constant. Figs. 3(a) and 3(b) elucidate a discernible decrease in

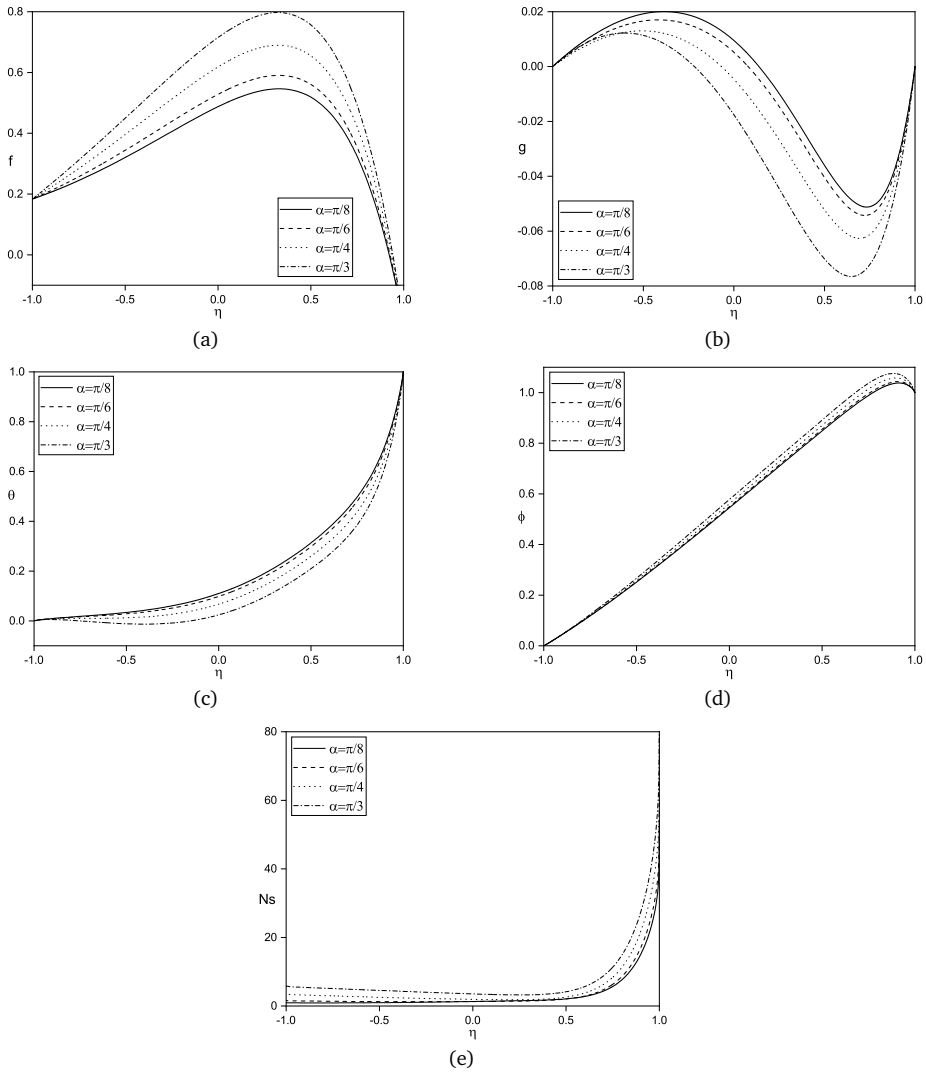

Figure 3: Effect of α on (a): $f(\eta)$, (b): $g(\eta)$, (c): $\theta(\eta)$, (d): $\phi(\eta)$, and (e): Ns.

both flow velocity and cross-flow velocity as the angle of inclination (α) experiences elevation. The behavior of temperature is depicted in Fig. 3(c). Here, an observable reduction in fluid temperature is noted with a rise in inclination angle (α). It is noted in Figs. 3(d) and 3(e) that as α rises, both fluid concentration and entropy generation exhibit augmentation. This is because as the inclination angle of the applied magnetic field changes (the angle of inclination increases), the reduction in drag force will subside on the net flow. An inclined magnetic field is used in MHD generators to convert the kinetic energy of hot, electrically conducting fluid into electrical energy.

In Fig. 4, the graphical representation elucidates the effect of the parameter γ on the variables f, g, θ, ϕ, and Ns, while maintaining constant values for other parameters: $\alpha = \pi/4, Sr = 2, Ha = 2, \lambda_1 = 0.5$, and $m = 2$. Figs. 4(a) and 4(b) exhibit contrasting trends.

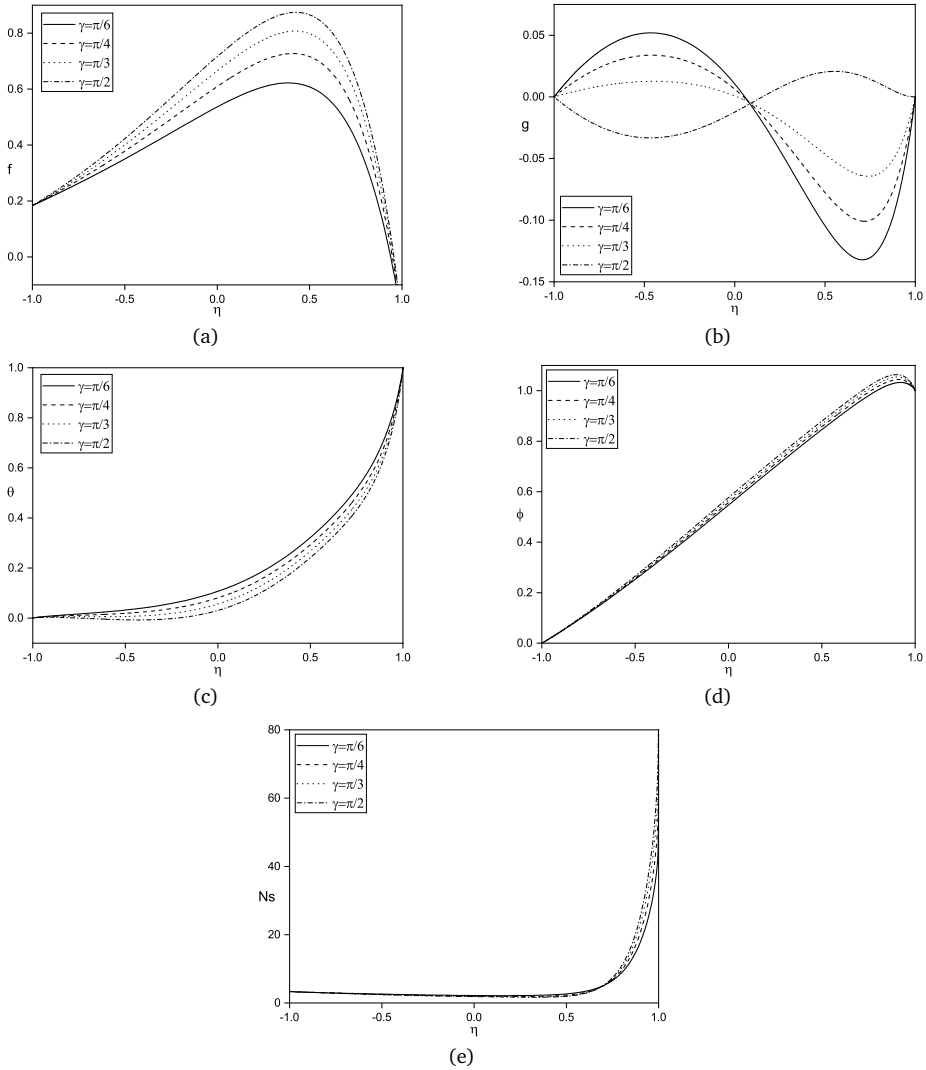

Figure 4: Effect of γ on (a): $f(\eta)$, (b): $g(\eta)$, (c): $\theta(\eta)$, (d): $\phi(\eta)$, and (e): Ns.

Specifically, the flow velocity demonstrates an ascending pattern, whereas the cross-flow velocity exhibits a descending trend as the parameter γ increases. This is because when the channel is inclined, a component of gravity acts along the channel direction. This component induces flow in an inclined direction due to the buoyancy force. The velocity increases as the inclined angle increases, leading to a higher flow rate in the direction of inclination. It is discerned that an elevation in the parameter γ leads to a fall in temperature and a simultaneous increase in fluid concentration, as depicted in Figs. 4(c) and 4(d). Entropy generation rises near $\eta = 1$ as m rises, as shown in Fig. 4(e). This phenomenon arises from the observation that as the angle γ increases towards 90°, the plates transition to a vertical orientation. Consequently, the magnetic field applied in this scenario induces a drag force in alignment with the y-axis direction.

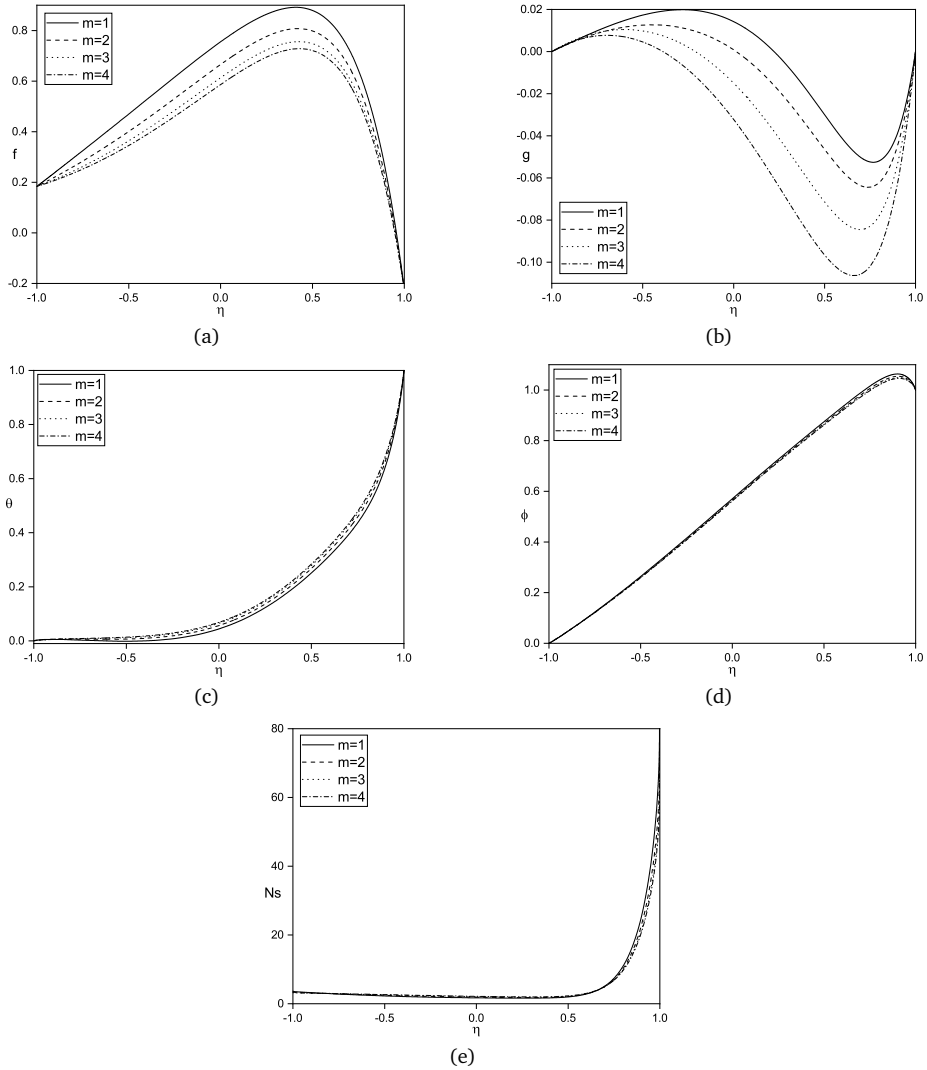

Figure 5: Effect of m on (a): $f(\eta)$, (b): $g(\eta)$, (c): $\theta(\eta)$, (d): $\phi(\eta)$, and (e): Ns.

Fig. 5 exemplifies the response of parameters f, g, θ, ϕ, and Ns to varying values of the Hall parameter (m), while maintaining constants for other parameters: $Sr = 2, Ha = 2, \lambda_1 = 0.5, \alpha = \pi/4$, and $\gamma = \pi/3$. As depicted in Fig. 5(a), a discernible reduction in flow velocity is observed with an escalation in m. It is seen from Figs. 5(b) and 5(c) that the cross-flow velocity and temperature both rise as m rises. When there is a magnetic field acting with an angle $\alpha = \pi/4$, Hall current will be generated perpendicular to both directions, which will act as a drag on flow velocity. Hall current generates an extra charge, which leads to an increase in the temperature of the fluid. The behaviors of fluid concentration and entropy generation near $\eta = 1$ are illustrated in Figs. 5(d) and 5(e), respectively. The concentration of fluid exhibits a rising trend, whereas entropy generation

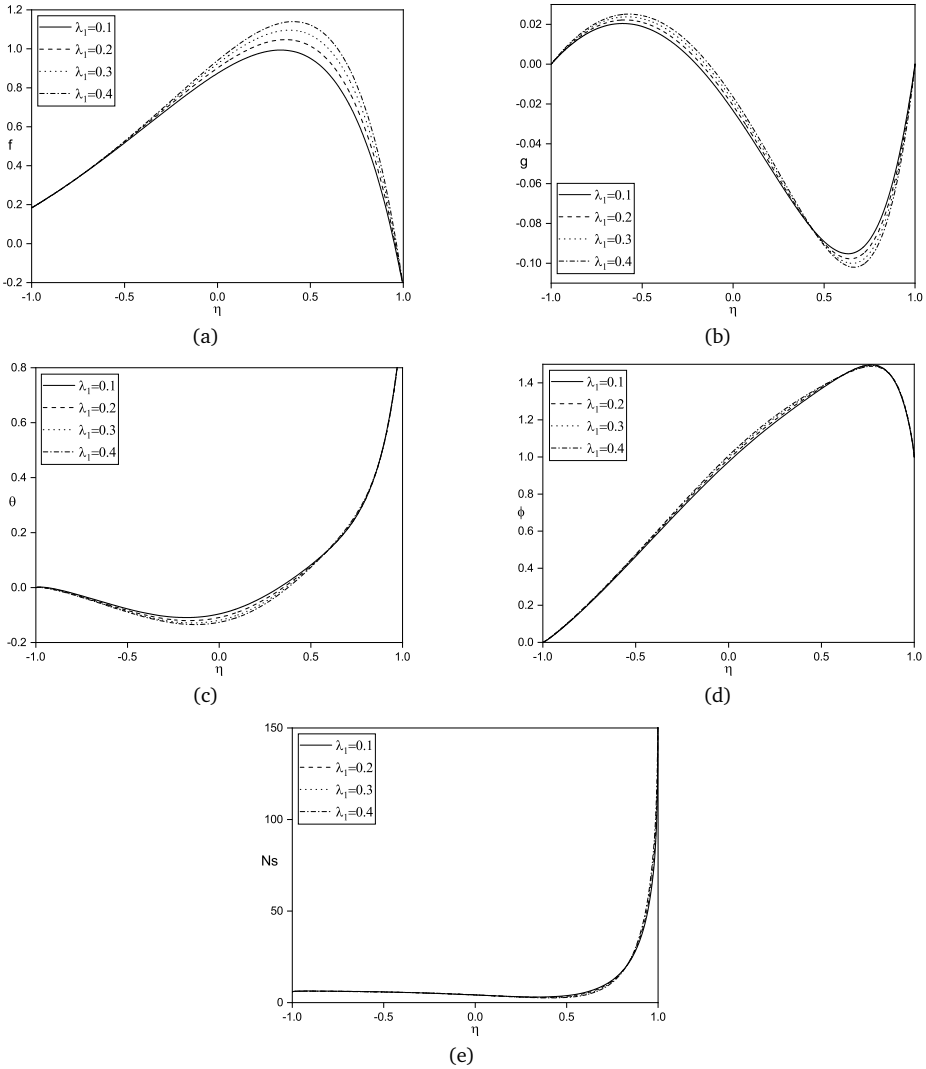

Figure 6: Effect of λ_1 on (a): $f(\eta)$, (b): $g(\eta)$, (c): $\theta(\eta)$, (d): $\phi(\eta)$, and (e): Ns.

decreases with an increase in the Hall parameter (m). Hall current induces mixing in the fluid flow. Mixing can lead to better dispersion of solute particles, influencing concentration gradients. Enhanced mixing due to the Hall parameter effect results in more uniform concentration profiles in the flow. The hall current plays a crucial role in MHD flows, introducing supplementary intricacy to both fluid dynamics and magnetic field dispersion. The realm of magneto-hydrodynamics (MHD) holds significance within plasma physics, astrophysics, and engineering domains, such as MHD power generation and propulsion systems, where the interplay of magnetic fields and fluid behavior is paramount.

The influence of λ_1 on f, g, θ, ϕ, and Ns is displayed in Fig. 6, while keeping other parameters at $Sr = 5, m = 2, \alpha = \pi/4, Ha = 2$, and $\gamma = \pi/3$. As delineated in Figs. 6(a)

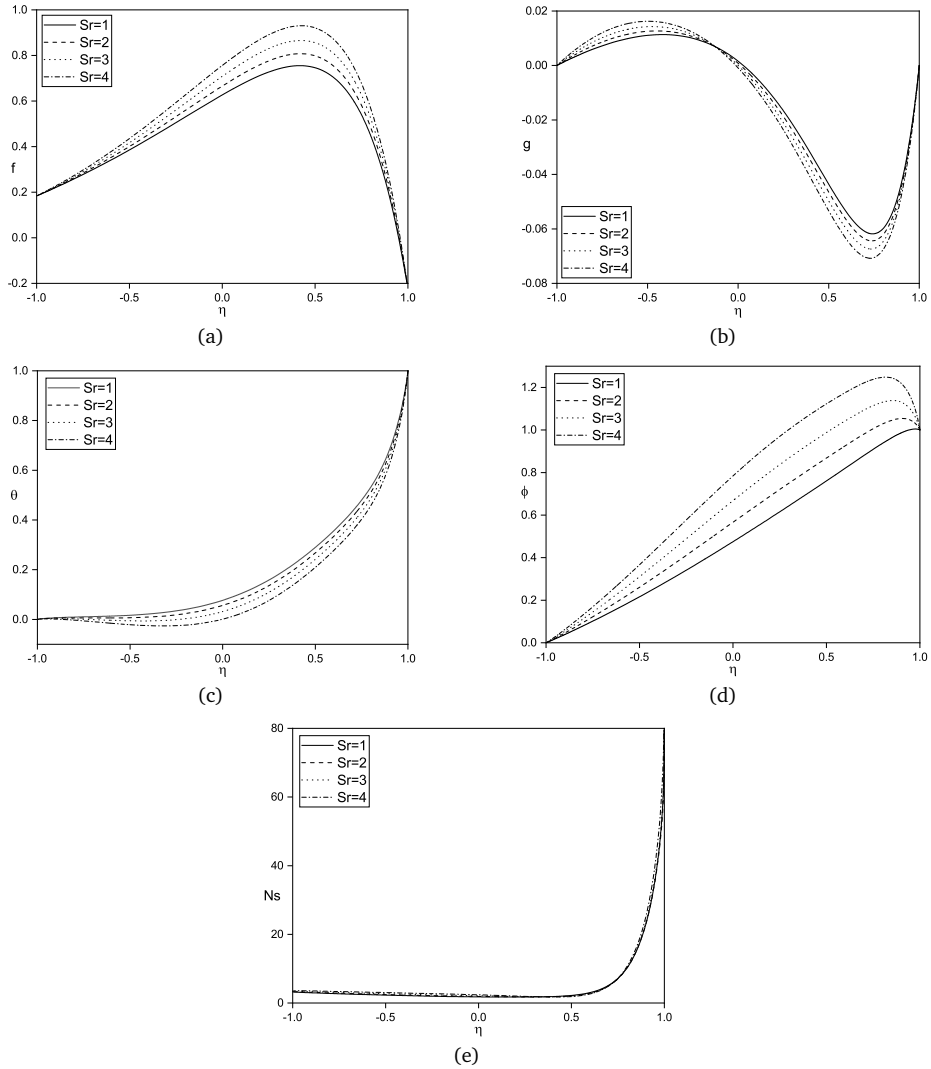

Figure 7: Effect of Sr on (a): $f(\eta)$, (b): $g(\eta)$, (c): $\theta(\eta)$, (d): $\phi(\eta)$, and (e): Ns.

and 6(b), as the parameter λ_1 increases, both velocity in the main flow direction and cross-flow velocity experience elevation. Higher values of the Jeffrey fluid parameter indicate more significant shear-thinning behavior. The shear-thinning behavior affects the flow profiles. As the fluid moves near the solid boundaries, where the shear rate is higher, a higher Jeffrey fluid parameter results in lower viscosity, allowing for faster flow. Fig. 6(c) shows that as the parameter λ_1 increases, the dimensionless temperature decreases. The behaviors of fluid concentration and entropy generation are portrayed in Figs. 6(d) and 6(e), respectively. Both parameters exhibit a positive trend with increasing λ_1. This implies that higher values of λ_1 contribute to elevated fluid concentration and a slight increase in entropy generation near $\eta = 1$. This is because the shear thinning behavior due to the

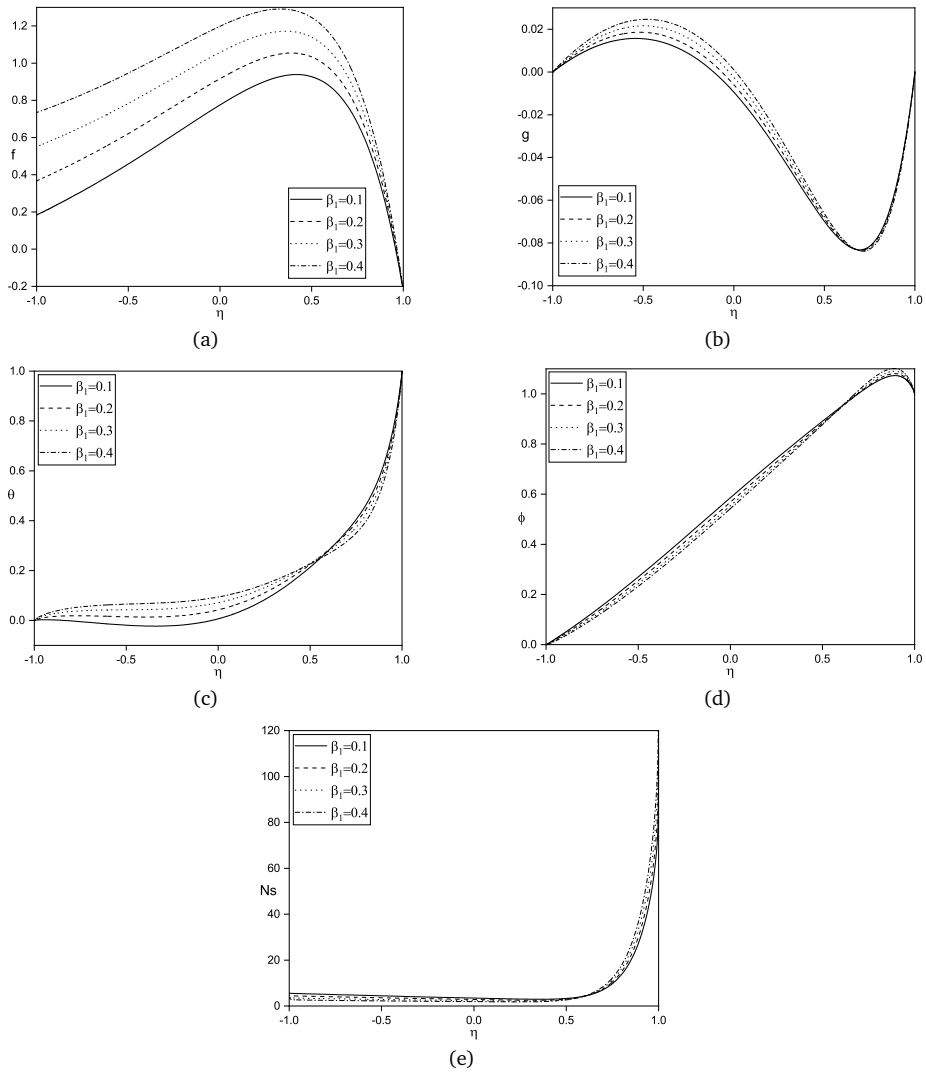

Figure 8: Effect of β_1 on (a): $f(\eta)$, (b): $g(\eta)$, (c): $\theta(\eta)$, (d): $\phi(\eta)$, and (e): Ns.

Jeffrey fluid parameter affects the thickness of the concentration boundary layer. A thinner boundary layer facilitates faster diffusion of solute particles, leading to an increase in the concentration profile.

In Fig. 7, the graphical depictions showcase the fluctuations in parameters f, g, θ, ϕ, and Ns in response to varying values of the Soret number (Sr), while $Ha = 2, m = 2, \alpha = \pi/4, \lambda_1 = 0.5$, and $\gamma = \pi/3$ are held constant. Figs. 7(a) and 7(b) illustrate that as the Soret number (Sr) escalates, both the flow velocity and cross-flow velocity exhibit an increase. The result in Fig. 7(c) indicates that the higher Soret numbers lead to lower fluid temperatures within the system. This phenomenon is attributed to the fact that an augmentation in the Soret parameter induces an escalation in the temperature gradient, consequently

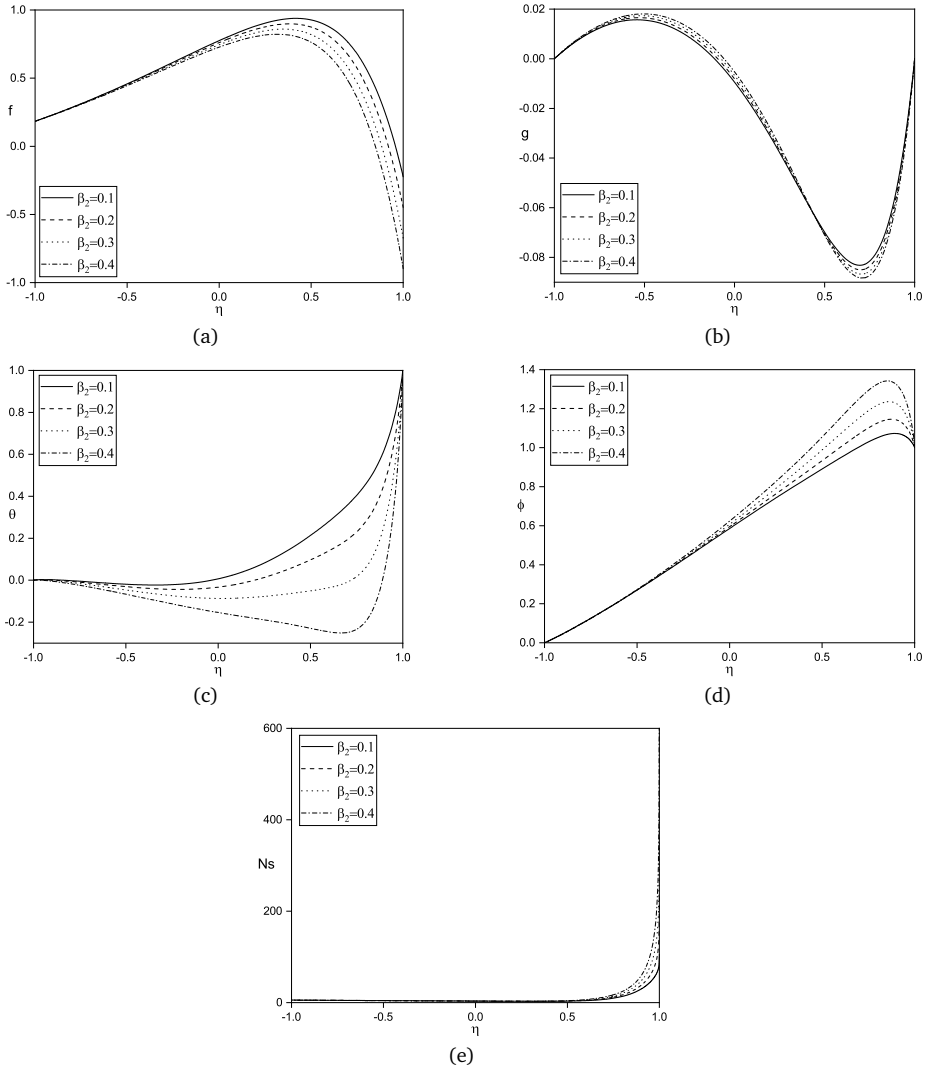

Figure 9: Effect of β_2 on (a): $f(\eta)$, (b): $g(\eta)$, (c): $\theta(\eta)$, (d): $\phi(\eta)$, and (e): Ns.

resulting in heightened velocities. Figs. 7(d) and 7(e) indicate that higher values of Sr contribute to elevated fluid concentration and entropy generation within the system. This happens because as the Soret parameter increases, the thermophoretic effect strengthens. Consequently, there is a greater mass flux of particles in response to a given temperature gradient. This effect can enhance mass transfer rates, leading to more rapid changes in concentration. This increased mass transfer results in higher entropy generation due to additional irreversibleness in the system.

In Fig. 8, the visualizations portray the responses of parameters f, g, θ, ϕ, and Ns to varying values of the parameter β_1, while keeping $Ha = 2, m = 2, \alpha = \pi/4, \lambda_1 = 0.5, Sr = 2$, and $\gamma = \pi/3$ constant. Figs. 8(a) and 8(b) demonstrate a noticeable pattern. Increasing the parameter β_1 is associated with higher values of both flow velocity and cross-flow velocity. This is because the fluid particles at the solid boundary are not anchored, allowing for easier movement and, consequently, higher velocity. Fig. 8(c) reveals that the temperature of the fluid rises with a rise in β_1. A higher slip leads to increased dissipation, affecting the overall temperature distribution in the flow. Figs. 8(d) and 8(e) demonstrate that higher values of β_1 contribute to reduced fluid concentration and entropy production within the system.

In Fig. 9, the graphical depictions present the variations in parameters f, g, θ, ϕ, and Ns corresponding to different values of the parameter β_2, while keeping $Ha = 2, m = 2, \alpha = \pi/3, \lambda_1 = 0.5, Sr = 2$, and $\gamma = \pi/3$ constant. Fig. 9(a) illustrates that an augmentation in the parameter β_2 is correlated with a decrease in the flow velocity. Fig. 9(b) shows that the cross-flow velocity increases as the value of the parameter β_2 rises. Fig. 9(c) reveals that the fluid temperature decreases as the parameter β_2 rises. An elevated slip results in greater dissipation, impacting the overall temperature distribution within the flow. The elevated value of the parameter β_2 corresponds to an increase in fluid concentration and a slight elevation in entropy production near $\eta = 1$, as depicted in Figs. 9(d) and 9(e). This occurs because when the fluid slips along the solid boundaries at $\eta = 1$, it can lead to heightened friction and shear within the boundary layer. These added dissipative effects result in increased entropy generation near $\eta = 1$.

Table 2 comprehensively depicts the fluctuations in various parameters such as the Jeffrey fluid parameter (λ_1), magnetic parameter (Ha), Soret number (Sr), Hall number (m), inclination angle (α), and channel angle of inclination (γ), while keeping other variables unchanged. The data in the table reveals that skin friction increases on the $\eta = -1$ plate and decreases on the $\eta = 1$ plate in sync with higher values of Ha, Sr, α, and channel inclination angle (γ), but decreases with increasing values of the Hall number (m). Conversely, skin friction reduces with higher values of the Jeffrey fluid parameter (λ_1). Table 2 also shows that as Ha, Sr, α, and γ increase, the heat transfer rate decreases for both plates. However, the Hall parameter (m) exhibits an opposite trend. Moreover, the rate of heat transfer increases on the left plate and decreases on the right plate with higher values of the Jeffrey fluid parameter (λ_1). Additionally, mass transfer rate increases with higher values of Ha, Sr, α, and γ, while exhibiting the opposite trend for m. The mass transfer rate decreases on the left plate and increases on the right plate with an increase in the Jeffrey fluid parameter (λ_1), as shown in Table 2.

Table 2: The skin friction coefficient, heat transfer, and mass transfer exhibit variations across discrete values of $\alpha, Sr, Ha, m, \gamma$ and λ_1, while considering the following parameters: $Re = 2, Gr = 2, Pr = 0.71, Br = 0.5, Sc = 0.22, N = 2, \beta_1 = 0.1$, and β_2=0.1.

Ha	Sr	m	α	λ_1	γ	Cf_1	Cf_2	Nu_1	Nu_2	Sh_1	Sh_2
1	2	2	$\pi/3$	0.2	$\pi/3$	0.22678	-3.38201	-0.29039	-7.67815	-0.34881	2.46179
2	2	2	$\pi/3$	0.2	$\pi/3$	0.37472	-3.81323	-0.42761	-8.58568	-0.28540	2.86414
3	2	2	$\pi/3$	0.2	$\pi/3$	0.59747	-4.32660	-0.62654	-9.67099	-0.19451	3.34504
2	1	2	$\pi/3$	0.2	$\pi/3$	0.35478	-3.63391	-0.42096	-8.15135	-0.30135	0.95933
2	2	2	$\pi/3$	0.2	$\pi/3$	0.37472	-3.81323	-0.42761	-8.58568	-0.28540	2.86414
2	3	2	$\pi/3$	0.2	$\pi/3$	0.39636	-4.01036	-0.43264	-9.07484	-0.26435	4.99950
2	2	1	$\pi/3$	0.2	$\pi/3$	0.55038	-4.22350	-0.58366	-9.45923	-0.21377	3.25147
2	2	2	$\pi/3$	0.2	$\pi/3$	0.37472	-3.81323	-0.42761	-8.58568	-0.28540	2.86414
2	2	3	$\pi/3$	0.2	$\pi/3$	0.28778	-3.58438	-0.34749	-8.10287	-0.32229	2.65006
2	2	2	0	0.2	$\pi/3$	0.06925	-2.80344	-0.14782	-6.33032	-0.41812	1.86217
2	2	2	$\pi/4$	0.2	$\pi/3$	0.37472	-3.81323	-0.42761	-8.58568	-0.28540	2.86414
2	2	2	$\pi/3$	0.2	$\pi/3$	0.48631	-4.21221	-0.50397	-9.58565	-0.24584	3.31009
2	2	2	$\pi/3$	0.2	$\pi/3$	0.48683	-4.61141	-0.45622	-9.64363	-0.26638	3.33607
2	2	2	$\pi/3$	0.3	$\pi/3$	0.48553	-5.01154	-0.41514	-9.69241	-0.28413	3.35786
2	2	2	$\pi/3$	0.4	$\pi/3$	0.48307	-5.41226	-0.37985	-9.73289	-0.29947	3.37586
2	2	2	$\pi/3$	0.2	$\pi/4$	0.43757	-3.91268	-0.44750	-8.23809	-0.27666	2.7111
2	2	2	$\pi/3$	0.2	$\pi/3$	0.45864	-4.21439	-0.45248	-8.83504	-0.27186	2.97646
2	2	2	$\pi/3$	0.2	$\pi/2$	0.48683	-4.61141	-0.45622	-9.64363	-0.26638	3.33607

6. Conclusion

The main objective of this study is to analyze the attributes of steady inclined magnetohydrodynamic mixed convection slip flow in a system of inclined parallel plates. This study employs a Jeffrey fluid model and considers the influence of both the Soret effect and Hall current. The non-dimensionalized equations are numerically solved using SQLM. The results obtained from such studies can be valuable for optimizing industrial processes, designing heat transfer systems, and improving energy efficiency in various engineering applications. The ensuing key discoveries stemming from this inquiry encompass:

1. When the Soret parameter (Sr), magnetic parameter (Ha), channel angle of inclination (γ), β_1, and Jeffrey fluid parameter (λ_1) increase, it increases fluid flow and cross-flow velocity. Conversely, the Hall parameter exhibits a reverse trend.

2. There is an increase in flow velocity and a decrease in cross-flow velocity as the inclination angle (α) increases, while the reverse tendency is seen in the β_2.

3. An increase in β_2, Soret parameter (Sr), magnetic parameter (Ha), inclination angle (α), channel angle of inclination (γ), and Jeffrey fluid parameter (λ_1) leads to

a decrease in temperature, while concentration experiences an ascent. Conversely, the trend is reversed for β_1 and the Hall parameter (m).

4. The entropy generation increases with the augmentation of the magnetic parameter (Ha) and inclination angle (α). Conversely, it diminishes as β_1 and the Hall parameter (m) experience an increase.

5. The skin friction coefficient displays an augmentation at the left plate and a reduction at the right plate in response to increases in Ha, Sr, α, and γ. Conversely, an opposite pattern is observed in the Hall parameter (m).

6. The heat transfer rate diminishes at both plates as the magnetic parameter (Ha), Soret number (Sr), inclination angle (α), and channel angle of inclination (γ) increase. Conversely, the mass transfer rate exhibits an opposite trend with the same parameters.

References

[1] A. Agrawal and J.P. Panda, *The Soret effect on MHD flow with Hall current and induced magnetic field*, Int. J. Ambient Energy **44(1)**, 450–462 (2023).

[2] G. Ali, F. Ali, A. Khan, A.H. Ganie and I. Khan, *A generalized magnetohydrodynamic two-phase free convection flow of dusty Casson fluid between parallel plates*, Case Stud. Therm. Eng. **29**, 101657 (2022).

[3] P. Bako and A.O. Ajibade, *G-Jitter effects on transient natural convection Couette flow in a vertical channel*, Int. J. Adv. Netw. Appl. **14(5)**, 5632–5644 (2023).

[4] K.S. Balamurugan, N.U.B. Varma and J.L.R. Prasad, *Entropy generation analysis on forced and free convection flow in a vertical porous channel with aligned magnetic field and Navier slip*, Heat Transf. **52(7)**, 4619–4639 (2023).

[5] R. Bellman, H. Kagiwada and R. Kalaba, *Quasilinearization, system identification and prediction*, Int. J. Eng. Sci. **3(3)**, 327–334 (1965).

[6] M. Bernatchou, K. Gueraoui, A. Rtibi, M. Cherraj and M. El Hamma, *Effect of magnetic field on double diffusive natural convection in an inclined cavity filled with nanofluid considering the Soret effect*, JP J. Heat Mass Transf. **25**, 1–25 (2022).

[7] A. Chamkha, M. Ismael, A. Kasaeipoor and T. Armaghani, *Entropy generation and natural convection of CuO-water nanofluid in C-shaped cavity under magnetic field*, Entropy **18(2)**, 50 (2016).

[8] A.J. Chamkha, C. Issa and K. Khanafer, *Natural convection due to solar radiation from a vertical plate embedded in a porous medium with variable porosity*, J. Porous Media **4(1)**, 69–77 (2001).

[9] S. Das, R.N. Jana and O.D. Makinde, *Magnetohydrodynamic mixed convective slip flow over an inclined porous plate with viscous dissipation and Joule heating*, Alexandria Eng. J. **54(2)**, 251–261 (2015).

[10] D. Dropkin and E. Somerscales, *Heat transfer by natual convection in liquids confined by two parallel plates which are inclined at various angles with respect to the horizontal*, J. Heat Transfer **87(1)**, 77–82 (1965).

[11] I. Filahi, M. Hasnaoui, A. Amahmid and M. Bourich, *Double-diffusive natural convection study in a shallow horizontal porous layer filled with a binary fluid and submitted to destabilized conditions in the presence of Soret effect*, Materials Today: Proceedings, Elsevier, **2021**, 7432–7437 (2021).

[12] T. Fujii and H. Imura, *Natural-convection heat transfer from a plate with arbitrary inclination*, Int. J. Heat Mass Transf. **15(4)**, 755–767 (1972).
[13] I.G. Gjerde and L.R. Scott, *Kinetic-energy instability of flows with slip boundary conditions*, J. Math. Fluid Mech. **24(4)**, 97 (2022).
[14] A. Hajizadeh, N.A. Shah, F.D. Zaman and I.L. Animasaun, *Analysis of natural convection bio-nanofluid between two vertical parallel plates*, Bionanoscience **9(4)**, 930–936 (2019).
[15] M.M. Hamza, G. Ojemeri and S.K. Ahmad, *Theoretical study of ARRHENIUS-controlled heat transfer flow on natural convection affected by an induced magnetic field in a micro-channel*, Engineering Reports e12642 (2023).
[16] T. Hayat and N. Ali, *Peristaltic motion of a Jeffrey fluid under the effect of a magnetic field in a tube*, Commun. Nonlinear Sci. Numer. Simul. **13(7)**, 1343–1352 (2008).
[17] T. Hayat, N. Ali and S. Asghar, *An analysis of peristaltic transport for flow of a Jeffrey fluid*, Acta Mech. **193**, 101–112 (2007).
[18] M. Junk and R. Illner, *A new derivation of Jeffery's equation*, J. Math. Fluid Mech. **9**, 455–488 (2007).
[19] K. Kaladhar, *Natural convection flow of couple stress fluid in a vertical channel with hall and joule heating effects*, Procedia Engineering **127**, 1071–1078 (2015).
[20] K. Kaladhar and M. Ravi, *Entropy analysis of natural convection Jeffrey fluid flow through a vertical channel with an inclined magnetic field effect under Navier-slip conditions*, Eur. Phys. J. Plus **138(8)**, 1–14 (2023).
[21] K. Kaladhar and M. Ravi, *Irreversibility mixed convection Jeffrey fluid flow analysis in a vertical channel with an inclined magnetic field and Soret effects under slip conditions*, Proc IMechE Part E: J Process Mechanical Engineering 1–12 (2023).
[22] D. Khan, K.K. Asogwa, T. Alqahtani, S. Algarni, S. Alqahtani and M.A. Akbar, *A generalized two-phase free convection flow of dusty Jeffrey fluid between infinite vertical parallel plates with heat transfer*, J. Math. **2022**, 101657 (2022).
[23] R. Kodi, R.R. Vaddemani, M.I. Khan, S.S. Abdullaev, A. Boudjemline, M. Boujelbene and Y. Bouazzi, *Unsteady magneto-hydro-dynamics flow of Jeffrey fluid through porous media with thermal radiation, Hall current and Soret effects*, J. Magn. Magn. Mater. **582**, 171033 (2023).
[24] B. Mandal, K. Bhattacharyya, A. Banerjee, A. Kumar Verma and A. Kumar Gautam, *MHD mixed convection on an inclined stretching plate in Darcy porous medium with Soret effect and variable surface conditions*, Nonlinear Eng. **9(1)**, 457–469 (2021).
[25] M. Mishra and J.P. Panda, *Soret effect for unsteady MHD mixed convective flow in porous medium with viscous dissipation*, Int. J. Ambient Energy **43(1)**, 5605–5615 (2022).
[26] H. Mondal, M. Almakki and P. Sibanda, *Dual solutions for three-dimensional magnetohydrodynamic nanofluid flow with entropy generation*, J. Comput. Des. Eng. **6(4)**, 657–665 (2019).
[27] S.S. Motsa, P.G. Dlamini and M. Khumalo, *Spectral relaxation method and spectral quasilinearization method for solving unsteady boundary layer flow problems*, Adv. Math. Phys. **2014**, Article ID 341964 (2014).
[28] S. Nadeem, S. Zaheer and T. Fang, *Effects of thermal radiation on the boundary layer flow of a Jeffrey fluid over an exponentially stretching surface*, Numer. Algorithms **57(2)**, 187–205 (2011).
[29] C.L. Navier, *Memoire sur les lois du mouvement des fluides*, Mem. Academie des Inst. Sci. Fr. **6**, 389–440 (1823).
[30] O. Ojjela, A. Raju and N. Naresh Kumar, *Influence of Induced magnetic field and radiation on free convective Jeffrey fluid flow between two parallel porous plates with Soret and Dufour effects*, J. Mech. **35(5)**, 657–675 (2019).
[31] E. Omokhuale and M.S. Dange, *Heat absorption effect on magnetohydrodynamic (MHD) flow*

of Jeffrey fluid in an infinite vertical plate, FUDMA J. Sci. **7(2)**, 45–51 (2023).

[32] M.I.A. Othman, K. Lotfy, S.M. Said and O. Anwar Beg, *Wave propagation in a fiber-reinforced micropolar thermoelastic medium with voids using three models*, Int. J. of Appl. Math. and Mechanics **8**, 52–69 (2012).

[33] D. Pal and S. Chatterjee, *Soret and Dufour effects on MHD convective heat and mass transfer of a power-law fluid over an inclined plate with variable thermal conductivity in a porous medium*, Appl. Math. Comput. **219(14)**, 7556–7574 (2013).

[34] D. Pal, S. Mondal and H. Mondal, *Entropy generation on MHD Jeffrey nanofluid over a stretching sheet with nonlinear thermal radiation using spectral quasilinearisation method*, Int. J. Ambient Energy **42(15)**, 1712–1726 (2021).

[35] A.H. Pordanjani, S. Aghakhani, A. Karimipour, M. Afrand and M. Goodarzi, *Investigation of free convection heat transfer and entropy generation of nanofluid flow inside a cavity affected by magnetic field and thermal radiation*, J. Therm. Anal. Calorim. **137(3)**, 997–1019 (2019).

[36] K. Raghunath, *Study of heat and mass transfer of an unsteady magnetohydrodynamic (MHD) nanofluid flow past a vertical porous plate in the presence of chemical reaction, radiation and Soret effects*, J. Nanofluids **12(3)**, 767–776 (2023).

[37] C.S. Reddy, B. Mahanthesh, P. Rana and K.S. Nisar, *Entropy generation analysis of tangent hyperbolic fluid in quadratic Boussinesq approximation using spectral quasi-linearization method*, Appl. Math. Mech. **42**, 1525–1542 (2021).

[38] D. Srinivasacharya, R. Bhuvanavijaya and B. Mallikarjuna, *Dispersion effects on mixed convection over a vertical wavy surface in a porous medium with variable properties*, Procedia Eng. **127**, 271–278 (2015).

[39] M. Tanveer, S. Ullah and N.A. Shah, *Thermal analysis of free convection flows of viscous carbon nanotubes nanofluids with generalized thermal transport: A Prabhakar fractional model*, J. Therm. Anal. Calorim. **144(6)**, 2327–2336 (2021).

[40] I. Tari and M. Mehrtash, *Natural convection heat transfer from inclined plate-fin heat sinks*, Int. J. Heat Mass Transf. **56(1-2)**, 574–593 (2013).

[41] H. Vaidya, C. Rajashekhar, G. Manjunatha, A. Wakif, K.V. Prasad, I.L. Animasaun and K. Shivaraya, *Analysis of entropy generation and biomechanical investigation of MHD Jeffery fluid through a vertical non-uniform channel*, Case Stud. Therm. Eng. **28**, 101538 (2021).

[42] K. Vajravelu, S. Sreenadh and P. Lakshminarayana, *The influence of heat transfer on peristaltic transport of a Jeffrey fluid in a vertical porous stratum*, Commun. Nonlinear Sci. Numer. Simul. **16(8)**, 3107–3125 (2011).

[43] G.C. Vliet, *Natural convection local heat transfer on constant-heat-flux inclined surfaces*, J. Heat Transfer **91(4)**, 511–516 (1969).

[44] F. Zare, M. Heydari, G.B. Loghmani, *Spectral quasilinearization method for the numerical solution of the non-standard Volterra integral equations*, Iranian Journal of Science **47(1)**, 229–247 (2023).